Thermal conductivity and particle agglomeration in alumina nanofluids: Experiment and theory

Elena V. Timofeeva, Alexei N. Gavrilov, James M. McCloskey, and Yuriy V. Tolmachev*
Department of Chemistry, Kent State University, Kent, Ohio 44242, USA

Samuel Sprunt
Department of Physics, Kent State University, Kent, Ohio 44242, USA

Lena M. Lopatina and Jonathan V. Selinger
Liquid Crystal Institute and Chemical Physics Interdisciplinary Program, Kent State University, Kent, Ohio 44242, USA
(Received 20 July 2007; published 28 December 2007)

In recent years many experimentalists have reported an anomalously enhanced thermal conductivity in liquid suspensions of nanoparticles. Despite the importance of this effect for heat transfer applications, no agreement has emerged about the mechanism of this phenomenon, or even about the experimentally observed magnitude of the enhancement. To address these issues, this paper presents a combined experimental and theoretical study of heat conduction and particle agglomeration in nanofluids. On the experimental side, nanofluids of alumina particles in water and ethylene glycol are characterized using thermal conductivity measurements, viscosity measurements, dynamic light scattering, and other techniques. The results show that the particles are agglomerated, with an agglomeration state that evolves in time. The data also show that the thermal conductivity enhancement is within the range predicted by effective medium theory. On the theoretical side, a model is developed for heat conduction through a fluid containing nanoparticles and agglomerates of various geometries. The calculations show that elongated and dendritic structures are more efficient in enhancing the thermal conductivity than compact spherical structures of the same volume fraction, and that surface (Kapitza) resistance is the major factor resulting in the lower than effective medium conductivities measured in our experiments. Together, these results imply that the geometry, agglomeration state, and surface resistance of nanoparticles are the main variables controlling thermal conductivity enhancement in nanofluids.

DOI: 10.1103/PhysRevE.76.061203 PACS number(s): 66.60.+a, 44.05.+e, 65.20.+w, 65.80.+n

INTRODUCTION

Over the past 15 years, many experimental studies have reported anomalous enhancement in the thermal conductivity of nanoparticle suspensions in liquids (known as nanofluids) compared to the same liquids without nanoparticles. Even though there had been earlier reports of such an effect [1], research in this area acquired a major thrust only after publications from a group at Argonne National Laboratory, who studied water- and oil-based nanofluids containing copper oxide nanoparticles, and found a striking 60% enhancement in thermal conductivity for only a 5% volume fraction of nanoparticles [2]. Since then, there have been similar reports of anomalous enhancement of the thermal conductivity of various nanofluids, using nanoparticles of oxides as well as of metals and carbon (for reviews, see Refs. [3–10]). Such enhancement of heat transport offers important benefits for numerous applications which rely on liquid coolants for carrying heat away from electronics or machinery.

Despite numerous studies stimulated by the fundamental and practical importance of this subject, it has proven rather difficult to establish either the magnitude or the mechanism of the thermal conductivity enhancement in nanofluids when following the early reports. Indeed, a recent review article has commented that "experimental values on the thermal conductivity of nanofluids published in the literature show an astonishing spectrum of results" [8]. Published results show enhancement in the thermal conductivity ranging from anomalously large values—i.e., much greater than the prediction of the classical Maxwell-Garnett effective medium theory—to values that are similar to or even less than the prediction of effective medium theory. Remarkably these discrepancies occur even for the same base fluid and the same nominal size and composition of the nanoparticles.

In addition to this range of experimental results, there is also a wide range of theoretical approaches for modeling thermal transport in nanofluids [11]. Some researchers have used variations of effective medium theory, involving nonspherical shapes [12–16] or a layer of ordered fluid around nanoparticles [14,17–21]. Other studies have considered thermal transport by the motion of nanoparticles, or convective thermal transport due to fluid flow entrained by nanoparticle motion [22–26]. The situation in the field has been recently described as "investigations of the properties of nanofluids have reached the awkward situation of having a greater number of competing theoretical models than systematic experimental results" [27].

The need for continuing studies to characterize individual nanofluid systems in greater depth, and to identify and correlate factors underlying their thermal conductivity, is therefore clear. In this paper, we present a combined, in-depth experimental and theoretical study of thermal conductivity of alumina (Al_2O_3) nanofluids, one of the most commonly studied yet still a controversial system (see Table 2) [1,2,28–39].

On the experimental side, we prepare nanofluids of Al_2O_3 particles in water and ethylene glycol, and characterize them

*Author to whom correspondence should be addressed.

with an unprecedentedly broad array of techniques, including thermal conductivity, viscosity and zeta-potential measurements, dynamic light scattering, and powder x-ray diffraction. The main experimental results are as follows:

(i) Our current experiments do not reproduce the anomalously high enhancements of thermal conductivity and the temperature dependence of the enhancement reported by other groups; our results are closer to the predictions of effective medium theory. This discrepancy may be associated with the differences in the shape and size of agglomerates as well as with the differences in particle-liquid and particle-particle heat transfer resistances on the surface and within agglomerates, respectively.

(ii) In the alumina nanofluids there is a significant nanoparticle agglomeration, as shown by the dynamic light scattering results as well as by viscosity measurements. Moreover, the agglomeration state of the particles evolves as a function of time, as the nanofluid ages (a process that is distinct from agglomerate sedimentation, which is carefully controlled in our experiments). Variations in the agglomeration state may well explain the variations in reported thermal conductivity in previous studies, which generally have not considered this phenomenon.

(iii) The crystal structure of the Al_2O_3 nanoparticles, obtained from commercial sources, varies significantly with nominal particle size, even from the same supplier, which complicates comparison of measured nanofluid properties. Furthermore, we find that the properties of nanofluids correlate better with the crystallite size (obtained from x-ray diffraction) than with nominal particle size (obtained from surface area measurements via gas sorption).

On the theoretical side, we estimate the rate of thermal transport through particle motion, and compare it with thermal transport due to heat diffusion through a static composite of particles and fluid. In the latter case, the particles may be spheres or nonspherical agglomerates, and they may have a finite surface thermal (Kapitza) resistance. The main theoretical results are as follows:

(i) Our calculations show that nanoparticle motion does not make a substantial contribution to thermal transport, compared with the diffusion of heat through static composites of nanoparticles and fluid.

(ii) However, the *geometry* of nanoparticles and particle agglomerates has a very important effect. Classical effective medium theory only applies to systems of spherical particles, and must be modified if the particles are elongated, or if they form agglomerates that are either elongated or dendritic (fractal). Earlier studies have considered certain elongated or fractal shapes, and have found a greater enhancement than for spheres. Here, we consider other shapes and confirm that a modified effective medium theory gives a greater enhancement in these cases. Furthermore, we show that the modified theory can account for previously published reports of anomalous enhancement in thermal conductivity.

(iii) Elongated and dendritic geometries can only explain thermal conductivity enhancements that are *greater* than effective medium theory for spheres. To explain thermal conductivity enhancements *less* than effective medium theory for spheres, such as those observed in the experiments reported below, we must consider thermal resistance at the nanoparticle-fluid interface. We show explicitly that our experimental results are consistent with an effective medium theory that includes interfacial thermal resistance.

Taken together, these experimental and theoretical results imply a unified picture of thermal conduction through nanofluids. In this picture, heat is transported diffusively through the composite, slowly through fluid and rapidly through particles and aggregates. For increasing the thermal conductivity of the composite one should consider (i) formation of extended particles or aggregates, (ii) enhancement of the orientational order of the particles or aggregates, and (iii) reduction of the surface resistance at the particle-liquid and particle-particle interfaces.

The plan of this paper is as follows. First we describe the experimental methods, followed by a detailed discussion of the experimental results. After that, we present a discussion incorporating the calculations for our theoretical model of nanofluids. Finally, in the Conclusions, we discuss implications of these results for future development of nanofluids for heat transport.

MATERIALS AND METHODS

The nanoparticles used in this work were Al_2O_3 with nominal diameters of 11 and 20 nm, made by Nanoamorphous Materials, and 40 nm Al_2O_3 NanoDur®, supplied by Alfa Aesar. The nominal sizes of the particles used throughout this work are the area-averaged sizes derived from gas sorption measurements reported by the manufacturers. We independently characterized the crystalline phases of the powders by x-ray diffraction performed on a D5000 diffractometer (Siemens) using a Cu-K_α x-ray source.

Purified water (Nanopure Diamond, Barnstead, with resistivity >18.2 M Ω cm^{-1} and <2 ppm of total organic carbon) and spectrophotometric grade ethylene glycol (99+%, Alfa Aesar) were used as the base liquids. Nanofluids with volume fraction of alumina from 0.5 to 10 vol % were investigated. The volume fraction of the powder was calculated from the weight of dry powder using the true density provided by supplier and the total volume of suspension. The manufacturer specified values (Table I), which agree closely with the reference values for γ-alumina (3.97 g/cm^2) and δ alumina (3.2 g/cm^2) [40], were used for true densities of alumina polymorphs through this work. Nanoparticles were dispersed into the base liquid and the mixture was sonicated continuously for 5 to 20 h in an ultrasonic bath (50 D, VWR). Even though the balance of gravitational and thermal energy [41] suggests that alumina nanoparticles smaller than 1 μm should be stable in water, some sedimentation was observed in aqueous nanofluids prepared from 11- and 20-nm alumina, possibly due to formation of large agglomerates. After sedimentation these suspensions were decanted and the new volume fraction of nanoparticles was determined by evaporation of an aliquot of the stable nanofluid at 90 °C followed by weighing of the dry residue. Nanofluids prepared from 40 nm particles were found to be stable in both water and ethylene glycol.

The effective thermal conductivity of nanofluids was measured using a thermal property analyzer (Model KD2pro,

TABLE I. Thermal conductivities of dry alumina powders.

Dry powders	True (bulk) density by manufacturer (g/cm^3)	Powder bulk density, experiment (g/cm^3)	Volume fraction (ϕ)	k_1^{exp} (W/m K)	$k_1^{cal}=k_1^{exp}/\phi$ (W/m K)
11-nm Al_2O_3	3.7 (0.1)	0.163	4.4%	0.0296	0.682
20-nm Al_2O_3	3.7 (0.16–0.4)	0.134	3.6%	0.0342	0.942
		0.275	7.4%	0.0320	0.431
40-nm Al_2O_3	3.6 (0.26)	0.469	13.0%	0.0433	0.330

Decagon Devices, Inc.), which is based on the transient hot wire method. The instrument's 60-mm long by 1.3-mm-diameter probe uses a folded platinum hot-wire line source in a stainless sheath fully immersed in the nanofluid. The electric current providing heat energy runs down and back along the probe coaxially, reducing electromagnetic effects on the nanoparticles near the probe that could be associated with transients when turning on and off of the electric current. Very low electrical powers (0.5 °C maximal temperature rise) were used to eliminate errors that could arise due to induced fluid convection. The probe temperature was recorded at 1-sec intervals both during application of electric current (while the probe temperature is increasing, 30 sec) and after removal of the current (probe temperature decreasing, 30 sec). The full set of data was analyzed using the heat diffusion equation solved for the cylindrical geometry appropriate to the sealed sample holder; no truncation of the data (e.g., to regimes where approximations to the diffusion equation solution might apply) was performed, reducing potential systematic errors. The outer wall of the sample holder was temperature controlled by fitting it snugly into a coaxial aluminum cylinder, which was suspended in a temperature regulated water bath (Isotemp 3016, Fisher Scientific, temperature stability <0.1 °C). The cylindrical sample cell dimensions were 10 mm radius by 70 mm length. The accuracy of the probe was carefully checked on pure water and ethylene glycol, and confirmed against literature values of the thermal conductivity of these liquids [42]. All measurements were performed ten times and averaged. The bias (for pure liquids) and the relative standard deviation of heat conductivity were typically less then 2% at room temperature. The viscosity of our nanofluid samples was measured using a Ubbeholder capillary viscometer (Fisher Scientific) at 23.0 ± 0.5 °C. *p*H measurements were carried out with UB-10 *p*H/mV meter (Denver Instruments) and a combination glass electrode (Orion), using commercial aqueous calibration solutions (Fisher Scientific). Zeta potentials of aqueous suspensions of Al_2O_3 diluted to 0.01% were measured using Zetasizer Nano (Malvern Instruments).

Agglomeration and the particle size distribution in nanofluids were studied with the dynamic light scattering (DLS) technique, conducted on samples contained in standard sealable optical cuvettes (Starna Cells, Inc., 1-mm path length) and at a 50° scattering angle on a home-built spectrometer. Samples were illuminated with vertically polarized, 633-nm light from a HeNe laser, and time correlation functions of the polarized scattered intensity were recorded with a digital correlator (Flexible Instruments model Flex2K-12Dx2) in the homodyne regime (with a typical signal to background ratio exceeding 90%). Intensity weighted particle size distributions were obtained by inverting the measured correlogram using commercial software (DYNALS, Alango, Ltd.). Specifically for the DLS experiments, nanoparticle suspensions were diluted to 0.1 or 0.01 vol %. Care was taken to eliminate effects of multiple scattering. In particular, studies of successively diluted suspensions were performed to establish a lower limit for detectable multiple scattering effects, and measurements were performed below this limit. In addition, the illuminated volume of the sample was imaged onto a selection aperture, which admitted to the detector only light scattered near the entry surface to the cell (where single scattering dominates).

EXPERIMENTAL RESULTS

Thermal conductivity of alumina powders

In order to estimate the intrinsic thermal conductivity of nanoparticles as well as particle-particle heat transfer resistance, we measured the thermal conductivity of solid alumina powders, k_1^{exp}. The same vial and probe were employed as for thermal conductivity of liquids. Powder density was also measured experimentally by weighing the vial of known volume after loading it with the powder. Our experimental results are shown in Table I along with the manufacturers' specifications for true and bulk powder densities. The volume fraction of the solid nanoparticles in the powder was calculated as the ratio of experimental bulk density to the manufactures' true density. The volume fraction varied between 3.6 and 13 %, depending on the type of the powder and how well it was compacted in the vial. Two different densities for 20-nm powder refer to loose and compact powder. It is worth noting that the volume fractions calculated this way fall in the same range as the volume fractions of nanofluids studied in this work. In order to estimate the true thermal conductivity of nanoparticles, k_1^{cal}, we divided the measured bulk thermal conductivity of the powder by the volume fraction of nanoparticles in the powder. This approach comes from the parallel cylinder model of porous media and it is oversimplified, as can be seen from the two different k_1^{cal} values found for the 20-nm powder. Nevertheless, it is useful for estimating the order of magnitude of k_1^{cal}. The values for the true thermal conductivity of nanoparticles fall in the range of 0.3–0.9 W/m K. These numbers are sig-

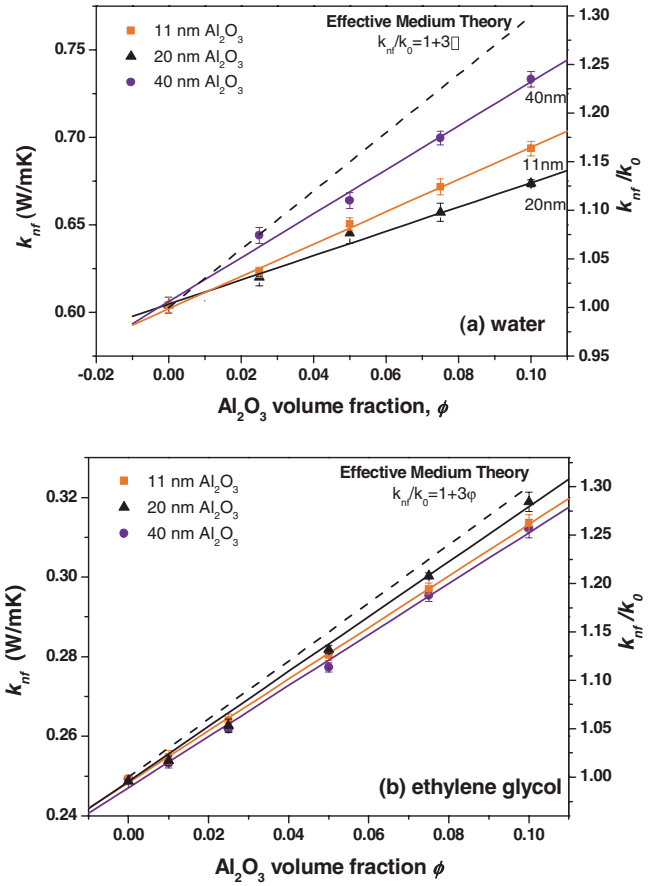

FIG. 1. (Color online) Thermal conductivity at 23 °C of suspensions prepared from 11-, 20-, and 40-nm nominal size alumina nanoparticles in (a) water and (b) ethylene glycol as a base fluid. The right axes show the enhancement effect relative to thermal conductivity of the base liquid. The dotted lines indicate predictions of the effective medium theory for spherical particles with infinite heat conductivity and $\phi \ll 1$. Error bars indicate standard deviation over ten consequent measurements.

nificantly below the 42 and 33–35 W/m K values reported for sapphire (single crystal α alumina) and even 18 W/m K accepted for polycrystalline α alumina [40]. We interpret this discrepancy as a clear manifestation of a large particle-to-particle heat transfer resistance in the powder.

Thermal conductivity of nanofluids

The nanofluid thermal conductivity k_{nf} as a function of nanoparticle volume fraction, ϕ for a series of Al_2O_3 nanofluids prepared from 11-, 20-, and 40-nm alumina powders and measured at 23 °C is presented in Fig. 1. The reduced conductivity is defined as k_{nf}/k_0, where k_0 is the thermal conductivity of the base liquid [water in Fig. 1(a) and ethylene glycol in Fig. 1(b)]. The thermal conductivity of the pure base fluids measured on our apparatus was found to be in excellent agreement with literature values. From Fig. 1, it can be seen that the thermal conductivity of nanofluids increases approximately linearly with ϕ. For aqueous nanofluids [Fig. 1(a)] the highest enhancement at any fixed volume fraction is observed in suspensions with particles of 40-nm nominal size, second highest for 11-nm particles, and smallest for 20 nm. The nonmonotonic trend with nominal particle size suggests complexity in the nanofluid system—e.g., the effect of different particle crystal structure on surface resistance to heat flow, different degrees, and nature of particle aggregation, etc.—to be discussed further below. By contrast, for ethylene glycol nanofluids [Fig. 1(b)], the nominal particle size does not have as significant an effect on the thermal conductivity enhancement, with all the results falling nearly on the same line.

In Table II we compare our present results for the thermal conductivity enhancement in Al_2O_3 nanofluids with corresponding data from other groups at the same volume fractions. This comparison shows that our results are at the lower end of the range of published values. Moreover, our experiments show a lower enhancement of the thermal conductivity than predicted by effective medium theory for spherical particles [6,9]. In this simple theory, the particles are assumed to be immobile. If the particles are spherical, the thermal conductivity of the particles is much greater than that of the fluid, and the volume fraction of nanoparticles is small, the prediction is

$$\frac{k_{\mathrm{nf}}}{k_0} = 1 + 3\phi.$$

For a volume fraction of 5%, this gives a thermal conductivity enhancement of 15%. Many of the published findings are "anomalously" above this level; however, our experimental findings are clearly lower. Our results in Fig. 1 also reveal that the same volume fraction of Al_2O_3 particles yields a higher thermal conductivity enhancement in ethylene glycol than in water. Similar observations were made previously [8,31], demonstrating that the enhancement is higher in the nanofluids with a lower thermal conductivity of the base liquid $[k_0(\mathrm{EG}) < k_0(\mathrm{H_2O})]$, as predicted by effective medium theory without the assumption of infinitely high thermal conductivity of the nanoparticle material [see Eq. (4) below] [6,9].

In water-based nanofluids, we observed an evolution in thermal conductivity or aging effect (Fig. 2), especially in suspensions with higher concentrations of nominally smaller (11- and 20-nm) nanoparticles. Once nanofluids were prepared (and decanted, if necessary), the thermal conductivity values changed from day to day. This was the case even though there was no subsequent evidence of sedimentation, and even when the samples were sonicated before every measurement. Reproducible values of the thermal conductivity were measured only on the fifth to seventh day after preparation. However, suspensions of 40-nm alumina in water as well as suspensions of all nanoparticles in ethylene glycol showed stable values right after the nanofluid preparation and sonication. The observed aging of water-based nanofluids can be accounted for by the dependence of their thermal conductivity on the structure of nanoparticle agglomerates. The formation of larger agglomerates upon aging can lead to a larger thermal conductivity, as discussed below.

TABLE II. Comparison of experimental heat transfer enhancements in alumina nanofluids reported in earlier literature and in the present study.

Researcher/ reference	Base fluid	Nominal Al_2O_3 particle size	Volume fraction	Thermal conductivity enhancement	Enhancement slope and temperature	Method
Masuda *et al.* [1]	water	13 nm	4.3%	33%	7.7	transient hot wire
Eastman *et al.* [2]	water	33 nm	4.3%	9%	2.1	transient hot wire
	EG		5.0%	18%	3.6	
Lee *et al.* [28]	water	38 nm	5%	12%	2.4 at room temperature	transient hot wire
	EG		5%	17%	3.4 at room temperature	
Wang *et al.* [29]	water	28 nm	5%	14%	2.8	steady-state parallel plates
	EG		5%	26%	5.2	
	pump oil		5%	12%	2.4	
	engine oil		5%	26%	5.2	
Xie *et al.* [30,31]	water	60.4 nm	5%	22%	4.4 at 25 °C	transient hot wire
	EG		5%	29%	5.8 at 25 °C	
	GLY		5%	27%	5.4 at 25 °C	
	pump oil		5%	38%	7.6 at 25 °C	
Das *et al.* [32]	water	38 nm	4%	8%	2.0 at 21 °C	temperature oscillation
				25%	6.25 at 51 °C	
Putra *et al.* [33]	water	131 nm	4%	25%	6.3 at 50 °C	steady-state parallel plates with convection
Wen and Ding [34]	water	27–56 nm	1.6%	10%	6.3 at 22 °C	transient hot wire
Nara *et al.* [35]	water	40 nm	0.5%	34%	68 at 85 °C	temperature oscillation
	EG			5%	10 at 85 °C	
	PG			0%	0 at 85 °C	
Chon *et al.* [36]	water	13 nm	1%	15%	15 at 60 °C	transient hot wire
		50 nm	4%	30%	7.5 at 70 °C	
		182 nm	1%	5%	5 at 60 °C	
Li and Peterson [37]	water	36 nm	6%	28%	4.6 at 36 °C	steady-state parallel plates
		47 nm	6%	26%	4.3 at 36 °C	
Krishnamurthy *et al.* [38]	water	20 nm	1%	16%	16 at room temperature	unspecified, possibly like Ref. [35]
Zhang *et al.* [39]	water	20 nm	5%	15%	3	transient hot wire
Present paper	water	11 nm	5%	8%	1.6	transient hot wire
		20 nm	5%	7%	1.3	
		40 nm	5%	10%	2.0	
	EG	all sizes	5%	13%	2.6	
					all at 10–60 °C	

Temperature dependence of thermal conductivity

Several groups have reported studies of the thermal conductivity enhancement at elevated temperatures [32,35,36,43]. Most of them reported an increase of the enhancement effect in nanofluids with temperature. We studied the temperature dependence of the thermal conductivity of water and ethylene glycol nanofluids with 5 vol % of 40-nm alumina particles. In the range from 10 to 65 °C, the absolute thermal conductivity increased. However, we also observed that this temperature dependence simply tracked the

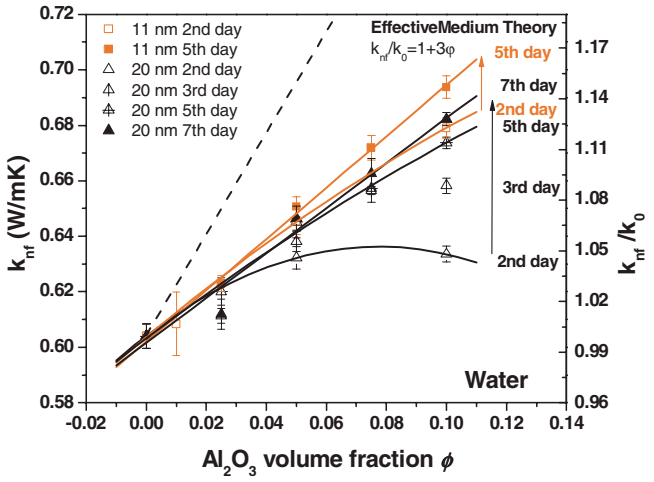

FIG. 2. (Color online) Effect of the aging in the water based nanofluids on the thermal conductivity.

temperature-dependent conductivity of the base fluid [42], which indicates that observed rise with increasing temperature comes from the base fluid rather than from behavior associated with the nanoparticles (Fig. 3). Thus we conclude that the enhancement in nanofluids *relative* to base fluids is essentially temperature independent.

Viscosity

Viscosity describes a fluid's internal resistance to flow, and, in the case of nanofluids, it depends on the morphology of the nanoparticles. We measured viscosities of a stable series of Al_2O_3/water and Al_2O_3/EG nanofluids with volume fractions from 0.5 to 10 % and nominal particle sizes 11, 20, and 40 nm using a capillary viscometer. Figure 4 shows the experimental data on the viscosities of nanofluids, η_{nf}, normalized to the viscosity of base fluid, η_0, with $\eta_r = \eta_{nf}/\eta_0$. In all cases, the results demonstrate that the viscosity dependence on particle volume fraction is stronger than the Einstein-Batchelor model for hard spheres [41], which predicts for $\phi \leq 0.10$

$$\eta_r \equiv \frac{\eta}{\eta_l} = 1 + 2.5\phi + 6.2\phi^2.$$

Suspensions of 40-nm alumina behave closest to the predictions of this simple model; this is presumably so because the particles in these solutions are more spherical in morphology. The deviations from the Einstein-Batchelor model observed in our work are similar to the results reported in Ref. [44] for 27-, 40-, and 50-nm Al_2O_3/propylene glycol nanofluids.

The viscosity values for the nanofluids with different nominal particle sizes follow trends similar to the trends observed for the thermal conductivities. The highest thermal conductivity was observed for the fluids with the lowest viscosity at the same volume fractions; i.e., the thermal conductivities increase in the sequence $k_{nf}(20\ \text{nm}) < k_{nf}(11\ \text{nm}) < k_{nf}(40\ \text{nm})$, while the viscosities decrease as $\eta_{nf}(20\ \text{nm}) > \eta_{nf}(11\ \text{nm}) > \eta_{nf}(40\ \text{nm})$. It is also apparent from Fig. 4 that water as a base liquid gives a larger deviation from the Einstein-Batchelor model than ethylene glycol. These large increases in viscosity for suspensions of 11- and 20-nm particles in water strongly indicate dendritic (fractal) agglomeration [41].

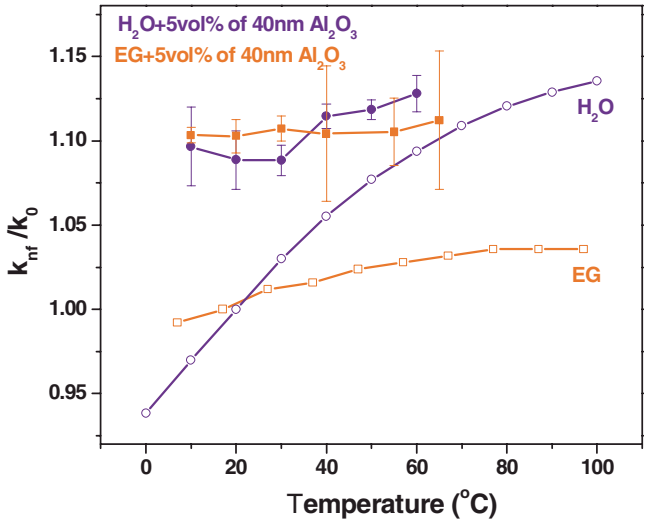

FIG. 3. (Color online) Effect of the temperature on the enhancement of thermal conductivity in nanofluids prepared with of 40-nm alumina (5 vol %) in water and ethylene glycol Curves with empty symbols show literature data for pure solvents. The data for pure liquids are normalized to their thermal conductivity at 23 °C and the data for nanofluids are normalized to the thermal conductivity of base fluids at the same temperature.

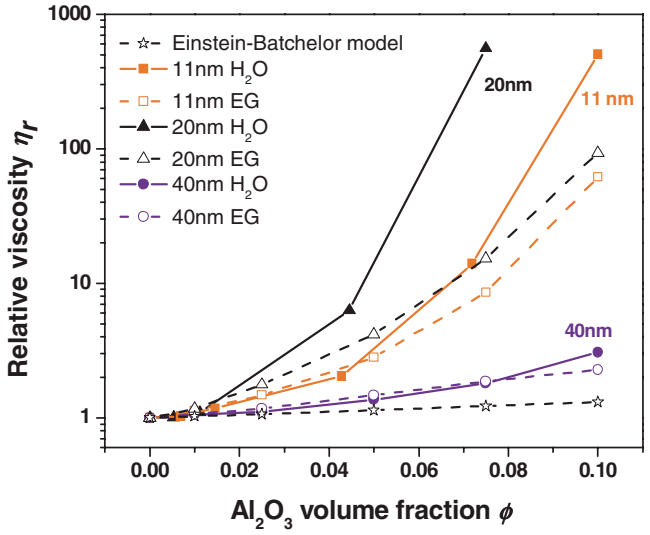

FIG. 4. (Color online) Relative viscosity changes of suspensions in water (solid line) and ethylene glycol (dashed line) as a function of alumina volume fraction at various nominal particle sizes. Black line with star symbols indicates the predictions of the Einstein-Batchelor model for solid spheres.

Dynamic light scattering

Since the viscosity data reveal compelling evidence of significant particle agglomeration, determination of the agglomerate size distribution is of primary importance for

proper interpretation of the thermal transport data. Dynamic light scattering (DLS) is a powerful and well-established technique that can be used to determine the size distribution of small particles in solution. By analyzing temporal correlation of the intensity scattered by thermal fluctuations of the particles in solution (Brownian motion), one can obtain the diffusion coefficients of the particles and then the hydrodynamic radii through the Stokes-Einstein equation. However, there are several limiting factors that must be considered. First, because there is a form factor associated with the scattered intensity from single particles that depends strongly on particle size, and because the shape or morphology of potentially agglomerated particles is not known *a priori*, the most reliable distribution extracted from the DLS data is a histogram of scattered intensity vs particle (or agglomerate) diffusion constant. To obtain a distribution in terms of an effective particle size, the shape of particles or agglomerates is assumed spherical and the Stokes-Einstein formula is applied to the diffusion constant. On the other hand, extracting a particle count vs size histogram is far more uncertain because of the extremely sensitive dependence of the form factor on unknown particle-aggregate morphology in solution. Hence we focus on intensity vs size histograms. A second caveat is that the Stokes-Einstein relation assumes noninteracting particles or aggregates. Finally, the inversion algorithms commonly used to extract size distributions from light scattering correlation data produce totally erroneous results when there is multiple scattering. As mentioned above, we therefore paid close attention to elimination of multiple scattering by using dilute solutions and detection optics that selectively admitted onto the detector singly scattered light from the illuminated sample volume.

For particle sizing, we diluted the same nanofluids used in the thermal conductivity and viscosity measurements to 0.1 and 0.01% volume fraction. Correlation functions for both concentrations coincide, which allowed us to conclude that there is no multiple scattering in 0.1% and that the dilution does significantly not influence particle-agglomerate sizes (not shown). Further analysis of 1, 2.5, 5, 7.5, and 10 % stable, aged suspensions diluted to 0.01% also showed no difference for samples prepared from the same nanoparticle powders.

Intensity-weighted distribution of agglomerate sizes for Al_2O_3 water-based nanofluids are represented in Fig. 5. In all cases, two peaks are observed: a smaller peak for smaller agglomerates (one to eight times larger than the nominal particle diameter d), and a bigger, broader peak for apparently larger agglomerates (hundreds of nanometers, typically ten or more nominal particles diameters). We also see that particles with the smaller nominal size (11 and 20 nm) form larger agglomerates, while particles with the larger diameter d (40 nm) form smaller agglomerates, apparently no larger than four times the nominal diameter. Stronger agglomeration of smaller alumina nanoparticles was observed previously by other researchers [2], who found that commercial alumina powders with much larger nominal sizes had more spherical shapes and showed better dispersion behavior in water than 3-nm alumina they prepared in the lab. Possible reasons for the stronger agglomeration of the smaller alumina particles may be their better ability to undergo

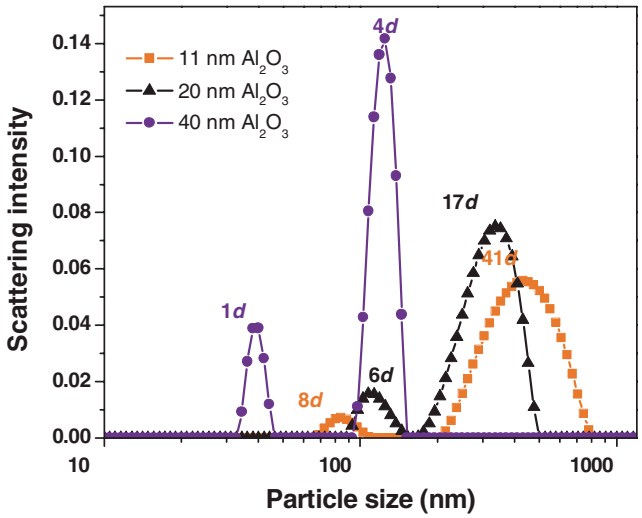

FIG. 5. (Color online) Scattering intensity vs effective size distribution for alumina nanoparticles and agglomerates in water (diluted to 0.01%) from dynamic light scattering measurements. The size of agglomerates is indicated in terms of the nominal particle size d.

dissolution-precipitation growth or their weaker repulsion due to a smaller surface charge, as discussed below. In the present work we confirm that particles with a larger nominal size give a more narrow distribution of particle sizes and that the peak is closer to the nominal size of the particles.

Comparison of DLS data for 11- and 40-nm Al_2O_3 nanofluids in water and ethylene glycol (Fig. 6) show agglomerate distributions centered on basically the same average sizes for suspensions made with particles of the same nominal d, but the distributions are narrower in the case of ethylene glycol. These results suggest that the particles are already agglomerated while in the powder, and that, apparently, only

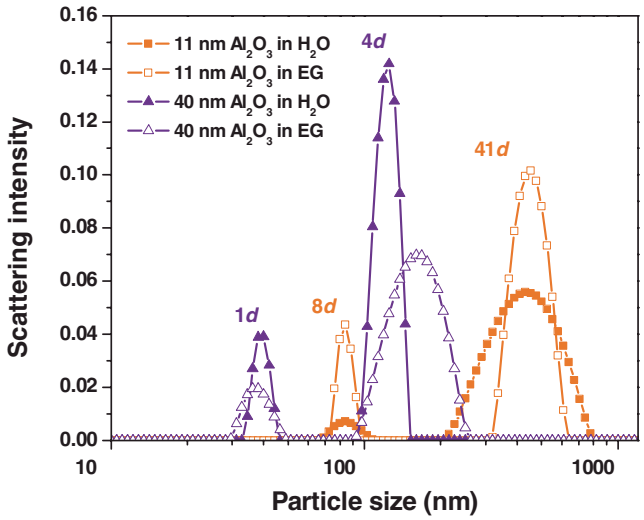

FIG. 6. (Color online) Size distributions of particles/agglomerates of nominal 10 nm (squares) and 40 nm (triangles) alumina formed in water (filled symbols) and ethylene glycol (empty symbols). The size of agglomerates is indicated in terms of the nominal particle size d.

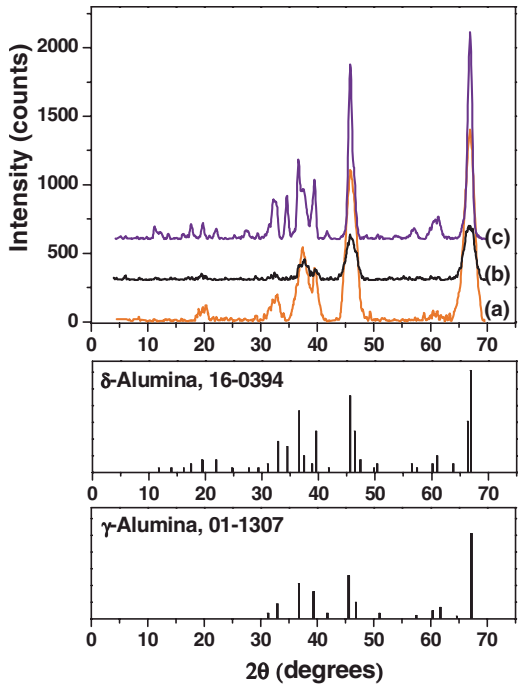

FIG. 7. (Color online) X-ray powder diffraction pattern of alumina nanoparticles: (a) 11-nm powder, (b) 20-nm powder, (c) 40-nm powder. Standard reference data for δ and γ aluminas are shown also. Compositions specified by manufacturers are 100% γ alumina for 11- and 20-nm powders and 70:30 mixture of δ:γ alumina for 40-nm powders.

the width of the agglomerate distribution changes significantly between the two solvents.

X-ray diffraction of alumina powders

The complexity of alumina nanofluids' behavior could be aggravated by the fact that aluminum forms an oxide, hydroxide, and many substances of intermediate composition (α, γ, δ, κ, η, θ and χ alumina) in the range $Al_2O_3 \rightarrow AlO(OH)$. Oxides and hydroxides have strong affinity for water and other polar molecules in general and readily adsorb a surface layer of water. The stability and adsorptive properties of aluminas depend on a combination of factors: crystal structure, pore size, surface structure, and it may also be affected by the presence of surface active sites, primarily OH^-, O^{2-}, and Al^{3+} ions [45,46].

Although some information was available from the suppliers, we carried out independent x-ray diffraction measurements with the alumina nanopowders used in our experiments. The x-ray diffraction (XRD) patterns presented in Fig. 7 indicate that while both the 10- and 20-nm nominally sized Al_2O_3 particles are composed of γ alumina, the "40-nm" powder consists of a roughly equal mixture of crystalline γ and δ alumina.

Approximate crystallite sizes can be determined by measuring the broadening of the x-ray diffraction peaks and applying the Debye-Scherrer equation [47]:

$$D_{vol} = 1.2\lambda/(B \cos \theta),$$

where λ is the wavelength of the x-ray source (1.5406 Å), B is the peak width, θ is the angle of the same peak, and D_{vol} denotes the volume-weighted crystallite diameter of the equivalent spherical particles. The experimental upper limit for size determination with the Debye-Scherrer equation is of the order of 100–200 nm [47].

TABLE III. Crystallite sizes of alumina nanopowders.

Alumina, nominal particle size	2θ	D_{vol} (nm)
11 nm	45.8	5.41
	67.0	5.77
20 nm	45.8	5.40
	67.0	5.27
40 nm	45.8	13.02
	67.0	12.00

The widths (defined as a ratio of peak area to peak height) of the most intense x-ray diffraction peaks have been used for the evaluation of the crystallite sizes. The calculated crystallite sizes for our alumina samples are 5.4–5.8 nm for nominal 11-nm alumina, 5.3–5.4 nm for 20-nm alumina, and 12.0–13.0 nm for 40-nm alumina, respectively (see Table III). However, these values should be treated with care since our calculations were performed without correction for instrumental and stress broadening. Nevertheless, the crystallite sizes estimated from powder XRD peak broadening show that the alumina particles are indeed two to five times smaller than their nominal particle size determined by manufacturers from surface area measurements. This discrepancy is likely due to the agglomeration of crystallites in the solid powders as was noted before based on dynamic light scattering data. It should be noted here that the degree of agglomeration determined from DLS, the increase in viscosity, and the enhancement in thermal conductivity show monotonic dependences on the actual XRD crystallite size rather that the nominal surface-area-based particle size. In the Discussion section, we will consider the possible impact of these basic structural differences on the heat transport in the corresponding nanofluids.

Nanofluid pH and zeta potentials

Surface chemical effects have only recently been considered as factors in the thermal conductivity of nanofluids. Xie *et al.* showed that simple acid treatment of carbon nanotubes enhanced their suspension stability in water [48]. This effect was attributed to hydrophobic-to-hydrophilic conversion of the surface due to the generation of a hydroxyl group. Lee *et al.* experimentally investigated the effect of surface charge state CuO nanoparticles in aqueous suspensions on the thermal conductivity [49]. They showed that the *p*H value of the nanofluid strongly affected the thermal performance of the fluid. As the *p*H value diverged from the isoelectric point (IEP), the particles acquired larger charge and particle-to-particle repulsion increased, thus making the suspension more stable. For reasons still not understood, the particles with a higher charge showed a greater enhancement of the thermal conductivity [49].

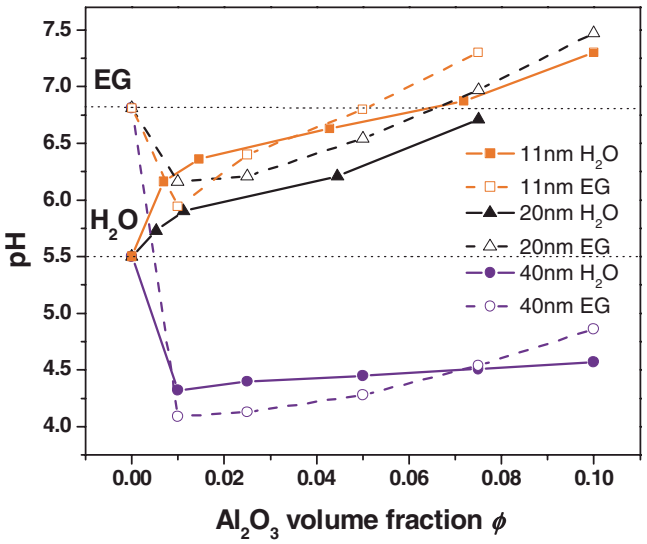

FIG. 8. (Color online) Equilibrium *p*H values of suspension in water (solid lines) and EG (dashed lines) at various volume fractions and nominal sizes of alumina nanoparticles. Dotted lines indicate *p*H values of base fluids.

We measured *p*H values of stable Al_2O_3 suspensions prepared in the same fashion as for our thermal conductivity measurements. Figure 8 displays the results. From the similarity of data obtained in water and ethylene glycol-based solutions, one can see that *p*H values in the suspensions depend on the structure and properties of the nanoparticles themselves, rather than on solid-liquid interactions. Water in contact with air has a *p*H of 5.5 resulting from some CO_2 dissolution from air, whereas ethylene glycol in contact with air has a *p*H of 6.8, close to neutral. IEPs reported for alumina are 7–8 for the γ phase and 8–9 for the α phase [30,50,51]. When 1 vol % of nominal 40-nm δ/γ-alumina nanoparticles are added to either solvent, the *p*H drops to 4.0–4.2. This could indicate the release of protons from the crystalline phase or high consumption of hydroxyl anions when alumina surface carries positive charge. On the other hand, for pure γ alumina (11- and 20-nm nominal size at 1.0 vol %), we observe smaller *p*H changes, falling into the gap between *p*H of pure water and ethylene glycol (Fig. 8). This difference can be attributed to a more acidic nature of δ alumina. This conclusion is also supported by the data on ionic conductivity of 0.1 vol % aqueous nanofluids (Table IV), which show an order of magnitude higher conductivity of 40-nm alumina suspension.

Increasing the volume fraction at the constant nominal particle size we increase the surface area of alumina in the contact with fluid. Experiments show that increase in volume fraction for all particle sizes shifts the *p*H to more basic values. The latter could explain why we observe different *p*H values in suspensions of the same γ alumina with nominal sizes 11 and 20 nm. For smaller particles the surface area at the same volume fraction is significantly higher. The higher *p*H values (close to IEP) result in the lower surface charge and weaker repulsion between particles, which leads to the stronger agglomeration in the case of smaller particles (11 and 20 nm), as observed by DLS. On the other hand, suspensions with a lower *p*H (40 nm), and thus with a higher surface charge, show significantly reduced agglomeration.

TABLE IV. Zeta potentials of alumina nanoparticles in 0.01 vol % suspensions in water, conductivities, and *p*H of the suspensions.

Nominal particle size	Zeta potential (mV)	Standard deviation (mV)[a]	Conductivity (mS/cm)	*p*H
11 nm	60.6	6.52	0.0021	6.47
20 nm	56.2	6.20	0.0029	5.55
40 nm	57.6	7.83	0.0279	5.03

[a]The standard deviations shown here represent the characteristics of the Gaussian distribution of zeta potentials obtained in a single experiment with a polydisperse nanofluid. It does not represent the reproducibility between independent experiments.

In order to assess the surface charge on alumina nanoparticles we performed zeta-potential measurements. Because of the limitations of the optical detection scheme used in our experiments, only diluted suspensions (0.01% vol) were studied. As shown in Table IV, all three types of nanoparticles show zeta potential of approximately +60 mV, despite the differences in *p*H of the nanofluids. Note that +60 mV is the limiting value of zeta potential for alumina nanoparticles at $pH < 7$, i.e., in solutions much more acidic than the IEP [52]. This suggests that all nanofluids used in our work contain highly positively charged alumina nanoparticles at all volume fractions studied. Even though we did not explicitly study the *p*H dependence of the heat transfer enhancement, our experimental conditions fall within the *p*H region where the maximal enhancement for alumina or water nanofluids was observed in previous reports [30].

Since alumina particles in our experiments carried high positive charge, we attempted to modify the surface charges of the nanoparticles by adding negatively charged citrate and chloride ions (as sodium and potassium salts, respectively) in concentration varying between 1 μM and 0.1 M. Both experiments produced negative results (in the sense of the thermal conductivity enhancement): when citrate was added to nanofluids, the particles agglomerated strongly, and the solid fraction settled down within an hour, leaving a clear base liquid. The addition of potassium chloride to the identical alumina suspension resulted in a huge rise of viscosity from milklike to creamlike consistency, while thermal conductivity remained the same as for the nanofluid without any added salts. The viscosity increase suggests the formation of dendritic agglomerates.

Successful stabilization of alumina nanoparticles in concentrated suspensions was described in Ref. [53], where the authors developed dispersants with molecular architecture tailored to the amphoteric alumina surface and with a controlled length. A systematic investigation of the influence of these surfactants on the thermal conductivity could be a promising research direction.

Theoretical model and discussion

We have found that the enhancement in thermal conductivity of water and ethylene glycol-based Al_2O_3 nanofluids,

in which there is a substantial degree of particle agglomeration, is below the level expected from classical effective medium theory. This finding, together with the disagreement between our results and those from a number of previous reports on similar systems (which present anomalously high values of thermal conductivity k_{nf}), warrants a critical assessment of possible factors responsible for thermal conductivity enhancement.

To develop a theory for thermal conduction in nanofluids, the first essential issue is to identify the primary mechanism for heat transport. As noted in the Introduction, some studies have modeled heat transport using versions of effective medium theory. In these models, nanoparticles are assumed to be stationary or slowly moving, with the heat diffusing through the "effective medium" composed of particles and fluid. Because the thermal conductivity of solids is usually much greater than that of liquids, the particle-liquid–particle pathways can lead to faster heat conduction through the medium below the percolation threshold. In addition, some studies modeled heat transport based on the motion of nanoparticles. The particle motion may also entrain the motion of the fluid, which will carry even more heat. This heat transport may provide an alternative mechanism for the enhancement of thermal conductivity of nanofluids [22,23,43,54,55].

Of course, both of these mechanisms may contribute to the thermal conductivity enhancement in nanofluids; the question is their relative magnitudes. To estimate the order of magnitude for the enhancement in effective medium theory, we can use the classical prediction for highly conducting spherical particles, i.e.,

$$\frac{k_{nf}}{k_0} = 1 + 3\varphi. \tag{1}$$

With the thermal conductivity of water $k_0 = 0.6\ \mathrm{W\,m^{-1}\,K^{-1}}$, and the typical nanoparticle volume fraction $\phi = 0.05$, this equation gives the enhancement $k_{nf} - k_0 = 0.09\ \mathrm{W\,m^{-1}\,K^{-1}}$. To estimate the order of magnitude for thermal transport through nanoparticle motion, we can calculate $\Delta k_{particle} = DC_{particle}c$, where D is the diffusivity of the particles, $C_{particle}$ is the heat capacity of each particle, and c is the number of particles per unit volume of nanofluid. Equivalently, this estimate can be rewritten as $\Delta k_{particle} = DC_V\phi$, where C_V is the specific heat per volume of solid particle. The diffusivity is given by the Stokes-Einstein relation as $D = k_B T/6\pi\eta R$. Using the thermal energy $k_B T = 4 \times 10^{-21}$ J at room temperature, the viscosity of the water $\eta = 10^{-3}$ Pa s, and the radius $R = 10$ nm, we obtain $D = 2 \times 10^{-11}\ \mathrm{m^2/s}$. The highest specific heat capacity of the aluminum oxide polymorphs is $C_V = 3 \times 10^6\ \mathrm{J\,m^{-3}\,K^{-1}}$ (for the α phase, also known as corundum). Combining these values gives $\Delta k_{particle} = 3 \times 10^{-6}\ \mathrm{W\,m^{-1}\,K^{-1}}$ for the same volume fraction 0.05. Of course, this is just a rough estimate of the thermal conductivity enhancement associated with particle motion, and it does not include the heat transported by entrained fluid motion. Still, one must note that this value is four orders of magnitude smaller than the thermal conductivity enhancement expected from effective medium theory. Thus it seems unlikely that particle motion contributes significantly to the thermal conductivity enhancement in nanofluids. Rather, the enhancement must be understood by regarding the particles as effectively fixed (moving slower that heat diffusion), with heat diffusing through and around them.

In order to model the diffusion of heat through the suspension, we must consider a range of geometries. For that reason, we briefly review the classical Maxwell-Garnett theory for spherical particles, and then discuss how the predictions are modified by nonspherical geometries.

The classical Maxwell-Garnett theory considers a system that consists of the base fluid with the thermal conductivity k_0 and one spherical nanoparticle with the thermal conductivity k_1, as shown in Fig. 9(a). When a thermal gradient is imposed on the system, the temperature distribution in the fluid and in the spherical particle is described by the functions $T_0(\mathbf{r})$ and $T_1(\mathbf{r})$, respectively. In steady state, the temperature profiles obey Laplace's equation,

$$\nabla^2 T_0 = 0, \quad \nabla^2 T_1 = 0, \tag{2}$$

with the boundary conditions

$$T_0 = T_1, \quad k_0 \frac{\partial T_0}{\partial n} = k_1 \frac{\partial T_1}{\partial n}, \tag{3}$$

for the temperatures and the normal derivatives at the interfaces between the two media. The first of the boundary conditions implies that there is no resistance to heat transfer at the fluid-particle interface, and the second implies that the heat current is continuous across the interface. Solving these equations and averaging the results over a random distribution of particles, we obtain the effective thermal conductivity of the nanofluid correct to first order in ϕ [56].

$$\frac{k_{\mathrm{nf}}}{k_0} = 1 + \frac{3(k_1 - k_0)}{k_1 + 2k_0}\phi, \tag{4}$$

where ϕ is the particle volume fraction. If the particles are much more conducting than the base fluid, i.e., $k_1 \gg k_0$, this result reduces to Eq. (1). The result corresponding to Eq. (4) for a circular nanoparticle in a two-dimensional nanofluid is

$$\frac{k_{\mathrm{eff}}}{k_0} = 1 + \frac{2(k_1 - k_0)}{k_1 + k_0}\phi \approx 1 + 2\phi \quad \text{(in two dimensions)}, \tag{5}$$

which does not apply to our three-dimensional (3D) experiments but is useful for theoretical comparisons.

One should notice that the slope of 3 in Eq. (1) is specific for spherical particles. However, the nanoparticles studied experimentally are not necessarily spherical. Furthermore, our experimental results show that the particles in nanofluids agglomerate substantially. Even if the nanoparticles are spherical when initially prepared, the agglomerates will generally not be spherical. Thus it is essential to determine how nonspherical geometries change the prediction for the thermal conductivity enhancement.

Figure 9(b) shows a schematic illustration of the geometry of nanoparticle agglomerates. From this picture we can see that the agglomerates have two important geometrical features—they are elongated and they have a dendritic or fractal structure. Nanoparticle agglomerates will generally be

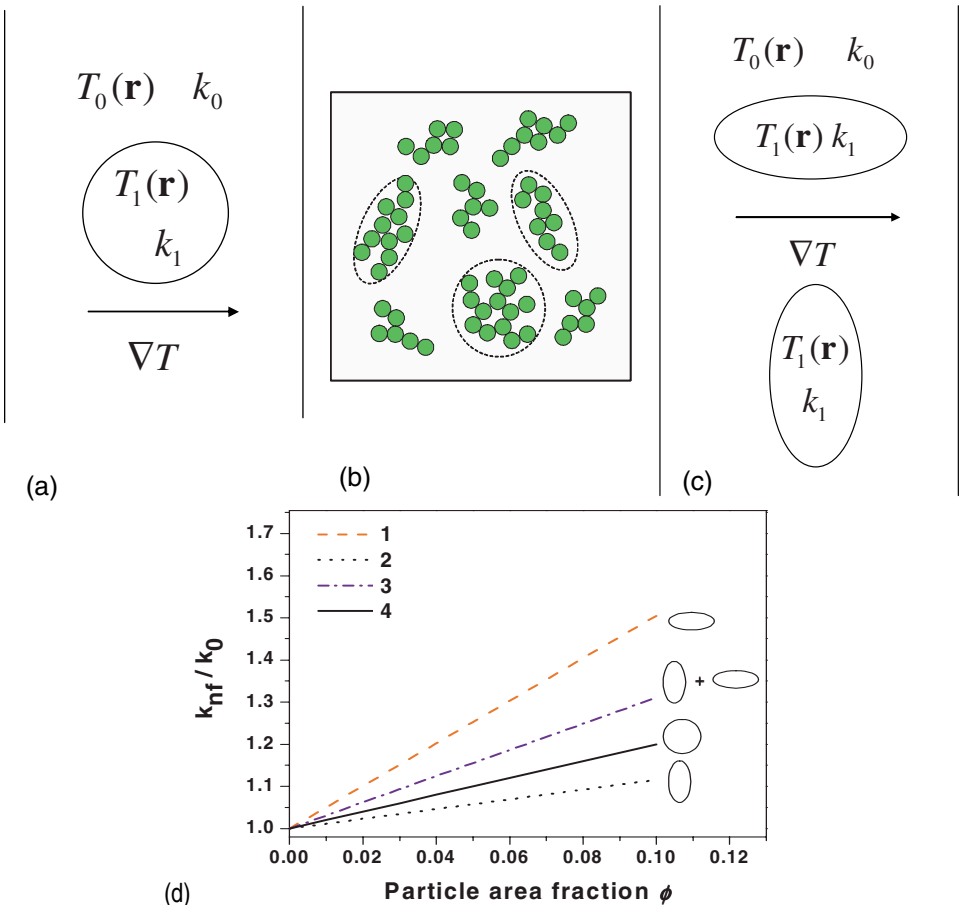

FIG. 9. (Color online) Theoretical modeling of the nanoparticle shape effect on the thermal conductivity of nanofluids within effective medium theory. Illustration of the temperature distribution problem for a sphere (a) and for an ellipse (c) in a fluid; (b) schematic representation of nanoparticle agglomerates; (d) averaged solution for different volume fractions of (1) ellipses oriented parallel to the temperature gradient; (2) ellipses oriented perpendicular to the temperature gradient; (3) isotropic distribution of the ellipse orientations; (4) effective medium theory for circles. The aspect ratio of the ellipses is 5:1.

elongated, merely because of the statistics of random clustering. For example, random-walk polymers typically have an aspect ratio of 3.4:1.6:1, compared with the spherical shape 1:1:1, as discussed in Ref. [57]. Elongated objects can transfer heat faster along the long axis. The dendritic or fractal structure of nanoparticle agglomerates is another important consideration, as has recently been pointed out by Prasher *et al.* [58]. Many types of formation conditions—such as diffusion-limited aggregation—lead to dendritic or fractal agglomerates, with complex rarified geometries of armlike dendrites separated by fluid interstices. Such structures can transport heat over long distances, characterized by a large radius of gyration. In that way, the nanofluids may act as if they had an effective volume fraction of nanoparticles that is much greater than the actual volume fraction. We can model each of these geometrical features separately.

Shape effects: Ellipses

In earlier research, other investigators have considered the effects of certain elongated shapes on the thermal conductivity of nanofluids. For example, Hamilton and Crosser considered cylindrical geometries [12], and Nan *et al.* considered ellipsoids and other 3D shapes [59]. Here, to see the effect of elongation in its simplest form, we consider 2D ellipses—either aligned or randomly oriented—and compare the results with the 2D prediction for circular disks.

The calculation for elliptical nanoparticles is analogous to the calculation above for circular nanoparticles, but with the geometry shown in Fig. 9(c). The temperature profiles again obey Laplace's equation [Eq. (2)], with the boundary conditions in Eq. (3) now applied to the boundary of an ellipse. Solving these equations for an ellipse with axes a along the gradient and b normal to the gradient gives the thermal conductivity enhancement:

$$\frac{k_{\mathrm{nf}}}{k_0} = 1 + \frac{(a+b)(k_1 - k_0)}{bk_1 + ak_0}\phi, \tag{6}$$

which is a generalization of Eq. (5) and is correct to first order in ϕ [56]. Reversing a and b gives the result for ellipsoids with long axes perpendicular to the temperature gradient. Equation (6) can be compared with calculations for three-dimensional ellipsoids by other methods [12,59].

This expression shows explicitly that the thermal conductivity of the system depends on the orientation of the elliptical particles with respect to the temperature gradient. As shown in Fig. 9(d) for ellipses with $a:b=5:1$, particles with long axes aligned parallel to the temperature gradient produce thermal conductivity enhancement much higher than predicted for circles. On the other hand, particles that are aligned perpendicular to the temperature gradient produce lower enhancement than predicted for circles. If we average over all possible orientations, representing an isotropic distribution of elliptical particles, we obtain the intermediate case also shown in Fig. 9(d). Note that this random distribution of orientations produces a greater enhancement than

predicted for circles: particle elongation enhances the thermal conductivity even if the particles are not aligned.

Shape effects: Dendrites

Apart from elongation, a further geometrical issue is how the effective thermal conductivity is affected by a dendritic (fractal) shape of the nanoparticle agglomerates. This is an important question, because agglomerating particles commonly form such structures. In such structures there are extended dendritic arms of highly conducting solid particles, separated by interstitial regions of the less conducting fluid. In the steady state, the fluid regions between the arms will have approximately the same temperature as the solid arms themselves. Hence the whole complex of nanoparticles plus interstitial fluid will function as a single effective particle from the perspective of enhancing the thermal transport. The volume taken up by such an effective particle can be much greater than the volume of the constituent nanoparticles themselves. We would expect the thermal conductivity enhancement to depend on the effective volume fraction of such agglomerates, rather than on the actual volume fraction of the particles. Thus thermal conductivity enhancement should be significantly greater for dendritic or fractal agglomerates than for isolated nanoparticles or compact agglomerates.

In a recent paper, Prasher *et al.* modeled the thermal conductivity of a nanofluid composed of fractal aggregates [15]. In this study, they used a specific model of the agglomeration process based on the model of cluster-cluster agglomeration, which gives rarified agglomerates with a fractal dimension $d_f = 1.8$. They calculated the thermal conductivity enhancement associated with such agglomerates, and showed that it is much larger than that for well-dispersed particles.

Here we would like to assess how general this result is. We would like to determine whether it depends on the specific model of cluster-cluster agglomeration, and indeed whether it depends on having agglomerates that obey fractal scale invariance, or if it is a general feature of disordered dendritic structures. For that reason, we calculate the thermal conductivity enhancement for simpler random structures, which are constructed by self-avoiding random walks of eight steps on a square lattice, as shown in Fig. 10(a). These structures are not truly fractal, but they have disordered shapes and dendritic arms, and hence can serve as models for experimental random agglomerates.

As an analytic solution of Laplace's equation in the presence of disordered particles is not feasible, we use a numerical approach to determine the temperature profile on a discretized lattice representing the nanofluid. For a disordered system, Laplace's equation for the temperature profile takes the form

$$\nabla[k(\mathbf{r})\,\nabla\,T(\mathbf{r})] = 0, \tag{7}$$

where $k(\mathbf{r})$ is the position-dependent thermal conductivity. We solve this equation on a 2D square lattice, where the temperature is defined on the lattice sites and thermal conductivities are defined on the bonds, as shown in Fig. 10(a). The temperature is fixed on two sides of the sample, creating a temperature gradient. Periodic boundary conditions are en-

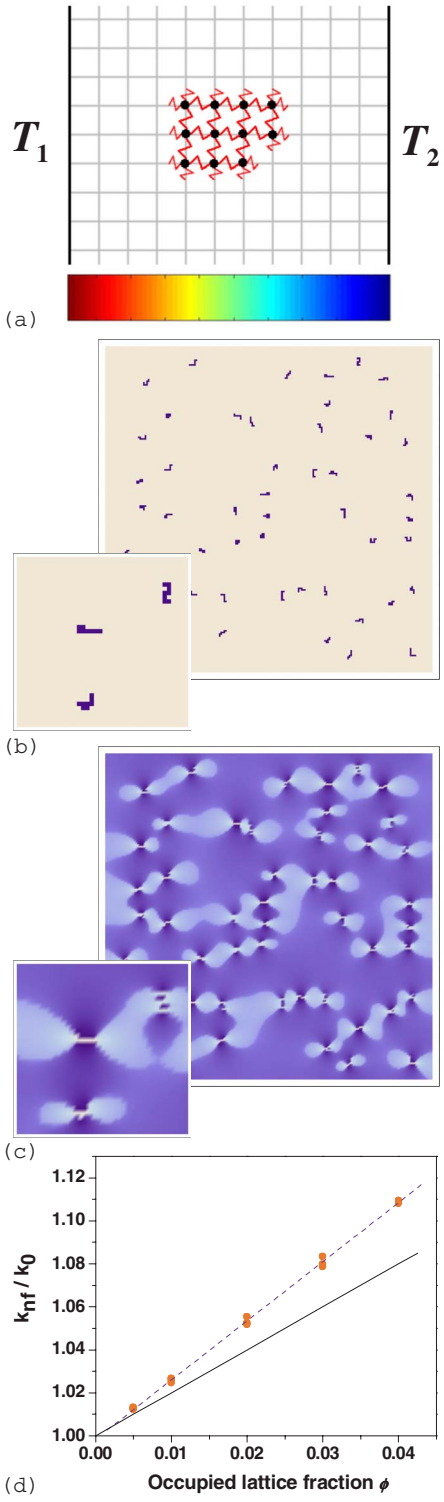

FIG. 10. (Color online) Theoretical study of the dendritic agglomeration effect: (a) illustration of the lattice geometry; (b) random distribution of the dendritic particles with 1% concentration; (c) calculated profile of the heat flux for the same distribution; (d) calculated thermal conductivity enhancement vs concentration of dendritic nanoparticles (dashed line with symbols) compared to circular nanoparticles (solid line) within effective medium theory. Three data points for each concentration shown in (d) correspond to three independent random distributions of particle shapes and positions.

TABLE V. Surface thermal conductance in alumina nanofluids.

Nominal particle size	Crystallite size (nm)	Slope in Fig. 1	Fitted $R\beta$ (W/m K)	β 10^8 W/m^2 K
40 nm in water	12.5	2.0	3.7	5.8
20 nm in water	5.3	1.3	1.1	4.0
11 nm in water	5.6	1.6	1.7	6.2
In ethylene glycol		2.6	4.5	

forced on the other two sides. To decrease computation time we use the alternating-direction implicit method [60]. For any random distribution of nanoparticle clusters, such as shown in Fig. 10(b), we solve Eq. (7) numerically to obtain the temperature profile. From this temperature profile, we obtain the heat flux and hence the average thermal conductivity.

The results can be analyzed in two ways. In Fig. 10(c), we show a visualization of the heat current through the sample, for a specific realization of the nanoparticle cluster distribution. This picture shows explicitly that the random clusters provide highly conducting paths for the heat. In the steady state, the system takes advantage of these paths by concentrating the heat current in the clusters, thereby enhancing the overall heat transport. In Fig. 10(d) we summarize numerical results for the effective thermal conductivity of the nanofluid with random-walk shaped agglomerates. For every particle concentration three independent realizations of shapes and positions of cluster were tried with no significant effect on the calculated thermal conductivities. The thermal conductivity enhancement varies linearly with the occupied lattice fraction, and with a higher slope than predicted from analytic solution for circular nanoparticles (5), shown by the solid line. Thus dendritic structures provide another mechanism for enhancing the thermal conductivity beyond the classical prediction.

Effect of surface thermal resistance

So far we have studied suspensions of elliptical nanoparticles (or elliptically shaped aggregates), as well as random dendritic or fractal nanoparticle aggregates. All of these cases show a *higher* effective thermal conductivity than predicted for spherical or circular nanoparticles dispersed in the base fluid. These theoretical results are consistent with experimental results of many research groups, as outlined in Table II, which often show a thermal conductivity enhancement beyond the classical prediction. However, our own experimental results, reported earlier in this paper, show a thermal conductivity enhancement that is somewhat *lower* than the classical prediction. To explain this smaller enhancement in the thermal conductivity, we cannot rely on geometrical effects. Rather we must consider the surface thermal resistance between the base fluid and the nanoparticles, as has been done in Refs. [22,59,61,62], and compare the results with experimental data.

To see the effect of surface thermal resistance, we can perform a calculation for a spherical nanoparticle with a resistive interface by analogy with our calculation above for a perfectly conducting interface. The system still obeys Laplace's equation (2) for the temperature, and the boundary condition (3) for the temperature gradients still applies. However, the boundary condition (3) for the temperatures is now changed to

$$T_0 - T_1 = \frac{k_0}{\beta}\frac{\partial T_0}{\partial n}, \tag{8}$$

where β is the surface thermal conductance, the inverse of the surface thermal resistance. When $\beta \to \infty$, this boundary condition reduces to the equality of temperatures across a perfectly conducting interface. By solving Laplace equation with this new boundary condition, and averaging the results over a uniform distribution of 3D spherical nanoparticles, we obtain a prediction for the thermal conductivity enhancement:

$$\frac{k_{\mathrm{nf}}}{k_0} = 1 + \frac{3(k_1 - k_0)}{k_1 + 2k_0 + 2k_0k_1/(R\beta)}\phi \tag{9}$$

consistent with Refs. [22,59,61,62] in the limit of small volume fraction. Note that this prediction depends on the radius R of the nanoparticles, unlike all the predictions above for nanoparticles with no thermal resistance, which depend only on the volume fraction.

We fit the experimental data of Fig. 1 to this prediction, in order to extract the composite parameter $R\beta$ that enters the equation. The results of this fitting are shown in Table V. Note that in the case of aqueous nanofluids the fitted parameter $R\beta$ does not follow a consistent trend with the nominal particle size, however, it does increase monotonically with the crystalline sizes determined from powder XRD. Moreover, the values of β for all particle sizes are about the same if crystallite sizes, D_{vol}, is used as $2R$, i.e., $\beta = 5 \times 10^8$ W/K m^2 for alumina-water interface. This value is at the high end of the values reported for metal nanoparticle-water interfaces [63]. Thus the simple classical model incorporating surface resistance reasonably accounts for the relatively low thermal conductivity enhancement in our experiments.

At this point we can ask why the thermal conductivity enhancement in alumina-water nanofluids correlates with crystallite particle size but not with surface-area averaged particle size nor with the size of agglomerates. More specifically, we need to explain why the least agglomerated 40-nm alumina nanofluids show the highest heat transport and the lowest viscosity enhancement, whereas 20-nm nanofluids show the lowest heat transport and the highest viscosity enhancement, with 11-nm nanofluids exhibit an intermediate behavior.

Despite the variety of techniques employed, our data are insufficient to provide a definite answer. Nevertheless, having identified the main factors in heat transfer enhancement

in nanofluids—the particle shape and the surface resistance—we can suggest the following scenario.

The 40-nm particles, due to the presence of acidic δ phase, are highly charged and do not undergo significant agglomeration in solution, as confirmed by viscosity, DLS, and the aging experiments (not shown in Fig. 2). This leads to the behavior closest to the ideal spherical particle case given by Eq. (1). The slightly smaller than ideal slope can be accounted for by the finite surface heat-transfer resistance (high $\beta \Rightarrow$ low $1/\beta$). Note that an earlier work reported identical heat transfer enhancement for α- and γ-alumina particles of the same specific surface area [30]. On the other hand, the more agglomerated 11-nm and 20-nm alumina nanofluids are expected to produce a higher enhancement than nanofluids with spherical particles. The viscosity data (Fig. 4) and the aging experiments (Fig. 2) suggest that the 20-nm nanofluids are the most agglomerated. This may be due to the presence of smaller alumina crystallites in this sample (as indicated by XRD), which makes it more prone to agglomeration via the dissolution-precipitation mechanism. The question now becomes why the more agglomerated nanofluids show a weaker heat transport enhancement than the less agglomerated, contrary to the theoretical considerations given above. It is possible that the heat-transfer resistance between the crystallites (and therefore between nanoparticles) within the agglomerate plays a critical role here. If this particle-particle resistance is large, it effectively eliminates the enhancement due to agglomeration and leads to the situation described by Eq. (9) with R being the radius of the crystallites in the agglomerate. This hypothesis is supported by the correlation of the heat transfer enhancement with the crystallite size and the consistency of β under this assumption (Table V), as well as the data on the thermal conductivity of the nanoparticle powder (Table I).

One further issue, which also requires an explanation, is why there is no particle-size effect in ethylene glycol nanofluids, while there is a strong particle size effect in aqueous nanofluids. Agglomeration is not likely to account for this difference, because the state of agglomeration in ethylene glycol and aqueous nanofluids is quite similar (see Fig. 6). However, we can explain all the experimental data in terms of the base fluid thermal conductivity k_1 and the interfacial thermal resistance β^{-1}. The base fluid thermal conductivity of ethylene glycol is about 2.4 times lower than that of water. Furthermore, we can hypothesize that the interfacial thermal resistance β^{-1} of nanoparticles in ethylene glycol is lower than that of the same nanoparticles in water. For those two reasons, the $2k_1/(R\beta)$ term in Eq. (9) would be much smaller in ethylene glycol nanofluids, and hence there would be no particle size effect. A lower interfacial thermal resistance also results in a higher slope of the thermal conductivity enhancement in ethylene glycol suspensions compared to water, as found in the experiments (see Table V). Unfortunately, the interfacial thermal resistance in the nanofluids studied in this work cannot be directly measured, and the proposed explanation still requires an independent confirmation. We also cannot give a simple account for a smaller interfacial thermal resistance in ethylene glycol compared to water, as such quantities do not always follow a simplified phonon spectra mismatch model, and they usually cannot be predicted based on rule-of-thumb arguments [64].

CONCLUSIONS

In this paper, we have presented an experimental and theoretical study of thermal conduction in nanofluids. In the experimental part of this work, we have investigated nanofluids of alumina in water and ethylene glycol, characterizing them through thermal conductivity measurements, dynamic light scattering, and other techniques. Our thermal measurements show that the thermal conductivity enhancement in our samples is within the range (actually somewhat lower than) predicted by effective medium theory for spherical particles. We do not find the anomalous enhancement reported by some other investigators. The absence of the temperature dependence of the enhancement also agrees with effective medium theory. Our experiments show that the nanoparticles are highly agglomerated, and that the agglomeration state varies in time as the sample ages. This observation suggests that the main reason why earlier investigations have given inconsistent results for the thermal conductivity enhancement is that they are examining systems with different distributions of agglomeration sizes and shapes. For that reason, it is very important that future experiments should characterize the agglomeration state of nanofluids carefully in direct correlation with thermal conductivity measurements.

In the theoretical part of this work, we have assessed possible mechanisms for thermal conductivity enhancement in nanofluids. By estimating characteristic magnitudes, we find that the contribution associated with nanoparticle motion is much smaller than the contribution associated with heat diffusion through the effective medium of particles and fluid, with the particles providing a path for rapid heat conduction. Furthermore, the geometry of nanoparticles and agglomerates plays a very important role in determining the thermal conductivity enhancement in effective medium theory. The prediction for compact spherical particles is the "worst case" for thermal conductivity—the enhancement is greater for extended elliptical particles, even randomly oriented ellipses, and the enhancement is also greater for dendritic or fractal aggregates. Thus there is no need to invoke theoretical mechanisms beyond effective medium theory to explain the anomalously high enhancement reported by other investigators; it is sufficient to consider effective medium theory for appropriate geometries and thereby to take into account higher "effective" volume fractions.

For improving thermal conductivity at fixed volume fraction, nanofluids should have extended particles or agglomerates, which can transport heat rapidly over significant distances within a sample. Ideally, these particles or agglomerates should be oriented with their long axes along the thermal gradient, in order to provide conducting paths in the optimum direction, as shown by our calculation for oriented ellipses. However, a related and equally important factor—which apparently plays the greater role in the alumina system studied here—is the heat transfer resistance at the particle-liquid interface, as well as interfacial resistance between the particles in the agglomerates, which must obviously be minimized. In our view, these factors should be the

primary focus for the continued development of nanofluids for thermal management applications.

ACKNOWLEDGMENTS

This research was supported by Office of Naval Research Grant No. N000140610029, the Ohio Board of Regents Research Challenge, and the National Science Foundation Research Experiences for Undergraduates Program. We would like to thank M. S. Spector for suggesting this project and for many helpful discussions.

[1] H. Masuda, A. Ebata, K. Teramae, and N. Hishinuma, Netsu Bussei **4**, 227 (1993).
[2] J. A. Eastman, U. S. Choi, S. Li, L. J. Thompson, and S. Lee, *1996 Fall Meeting of the Materials Research Society*, Boston, 2–6 Dec. 1996 (MRS, Pittsburgh, 1996), p. 1
[3] J. A. Eastman, S. U. S. Choi, S. Li, W. Yu, and L. J. Thompson, Appl. Phys. Lett. **78**, 718 (2001).
[4] J. A. Eastman, S. R. Phillpot, S. U. S. Choi, and P. Keblinski, Annu. Rev. Mater. Res. **34**, 219 (2004).
[5] P. Keblinski, J. A. Eastman, and D. G. Cahill, Mater. Today **8**, 36 (2005).
[6] S. K. Das, S. U. S. Choi, and H. E. Patel, Heat Transfer Eng. **27**, 3 (2006).
[7] M. J. Assael, I. N. Metaxs, K. Kakosimos, and D. Constantinou, Int. J. Thermophys. **27**, 999 (2006).
[8] S. Kabelac and J. F. Kuhnke, Annals of the Assembly for International Heat Transfer Conference 13, KN (2006).
[9] X. Q. Wang and A. S. Mujumdar, Int. J. Therm. Sci. **46**, 1 (2007).
[10] V. Trisaksri and S. Wongwises, Renewable Sustainable Energy Rev. **11**, 512 (2007).
[11] P. Keblinski, S. R. Phillpot, S. U. S. Choi, and J. A. Eastman, Int. J. Heat Mass Transfer **45**, 855 (2002).
[12] R. L. Hamilton and O. K. Crosser, I&EC Fundam. **1**, 187 (1962).
[13] B. X. Wang, L. P. Zhou, and X. F. Peng, Int. J. Heat Mass Transfer **46**, 2665 (2003).
[14] W. Yu and S. U. S. Choi, J. Nanopart. Res. **6**, 355 (2004).
[15] R. Prasher, W. Evans, P. Meakin, J. Fish, P. Phelan, and P. Keblinski, Appl. Phys. Lett. **89**, 143119 (2006).
[16] L. Gao and X. F. Zhou, Phys. Lett. A **348**, 355 (2006).
[17] W. Yu and S. U. S. Choi, J. Nanopart. Res. **5**, 167 (2003).
[18] L. Xue *et al.*, Int. J. Heat Mass Transfer **47**, 4277 (2004).
[19] Q. Xue and W. M. Xu, Mater. Chem. Phys. **90**, 298 (2005).
[20] H. Q. Xie, M. Fujii, and X. Zhang, Int. J. Heat Mass Transfer **48**, 2926 (2005).
[21] Y. J. Feng, B. M. Yu, P. Xu, and M. Q. Zou, J. Phys. D **40**, 3164 (2007).
[22] D. H. Kumar, H. E. Patel, V. R. Rajeev Kumar, T. Sundararajan, T. Pradeep, and S. K. Das, Phys. Rev. Lett. **93**, 144301 (2004).
[23] R. Prasher, P. Bhattacharya, and P. E. Phelan, Phys. Rev. Lett. **94**, 025901 (2005).
[24] J. Koo and C. Kleinstreuer, Int. Commun. Heat Mass Transfer **32**, 1111 (2005).
[25] Y. M. Xuan and Z. P. Yao, Heat Mass Transfer **41**, 199 (2005).
[26] P. Keblinski and J. Thomin, Phys. Rev. E **73**, 010502(R) (2006).
[27] S. A. Putnam, D. G. Cahill, P. V. Braun, Z. B. Ge, and R. G. Shimmin, J. Appl. Phys. **99**, 084308 (2006).
[28] S. Lee, S. U. S. Choi, S. Li, and J. A. Eastman, J. Heat Transfer **121**, 280 (1999).
[29] X. W. Wang, X. F. Xu, and S. U. S. Choi, J. Thermophys. Heat Transfer **13**, 474 (1999).
[30] H. Q. Xie, J. C. Wang, T. G. Xi, Y. Liu, F. Ai, and Q. R. Wu, J. Appl. Phys. **91**, 4568 (2002).
[31] H. Q. Xie, J. C. Wang, T. G. Xi, Y. Liu, and F. Ai, J. Mater. Sci. Lett. **21**, 1469 (2002).
[32] S. K. Das, N. Putra, P. Thiesen, and W. Roetzel, J. Heat Transfer **125**, 567 (2003).
[33] N. Putra, W. Roetzel, and S. K. Das, Heat Mass Transfer **39**, 775 (2003).
[34] D. S. Wen and Y. L. Ding, Int. J. Heat Mass Transfer **47**, 5181 (2004).
[35] S. Nara, P. Bhattacharya, P. Vijayan, W. Lai, P. Phelan, R. Prasher, D. Song, and J. Wang, in *2005 ASME International Mechanical Engineering Congress and Exposition* (Orlando, Florida, USA, 2005), p. 80524.
[36] C. H. Chon, K. D. Kihm, S. P. Lee, and S. U. S. Choi, Appl. Phys. Lett. **87**, 153107 (2005).
[37] C. H. Li and G. P. Peterson, J. Appl. Phys. **99**, 084314 (2006).
[38] S. Krishnamurthy, P. Bhattacharya, P. E. Phelan, and R. S. Prasher, Nano Lett. **6**, 419 (2006).
[39] X. Zhang, H. Gu, and M. Fujii, J. Appl. Phys. **100**, 044325 (2006).
[40] S. L. Phillips and D. L. Perry, *Properties of Inorganic Compounds* (CRC Press Inc., Boca Raton, FL, 2000).
[41] R. D. Vold and M. J. Vold, *Colloid and Interface Chemistry* (Addison-Wesley, Reading, MA, 1983).
[42] N. B. Vargaftik, L. P. Filipov, A. A. Tarzimanov, and E. E. Totskii, *Handbook of Thermal Conductivity of Liquids and Gases* (CRC Press, Inc., Boca Raton, 1994).
[43] S. P. Jang and S. U. S. Choi, Appl. Phys. Lett. **84**, 4316 (2004).
[44] R. Prasher, D. Song, J. Wang, and P. Phelan, Appl. Phys. Lett. **89**, 133108 (2006).
[45] J. C. Bailar, *Comprehensive Inorganic Chemistry* (Pergamon, Oxford, 1973).
[46] P. Patnaik, *Handbook of Inorganic Chemicals* (McGraw-Hill, New York, 2002).
[47] B. D. Cullity, *Elements of X-Ray Diffraction* (Addison-Wesley, Reading, MA, 1978).
[48] H. Q. Xie, H. Lee, W. Youn, and M. Choi, J. Appl. Phys. **94**, 4967 (2003).
[49] D. Lee, J. W. Kim, and B. G. Kim, J. Phys. Chem. B **110**, 4323 (2006).
[50] J. P. Brunelle, Pure Appl. Chem. **50**, 1211 (1978).
[51] M. Haruta, J. New Mater. Electrochem. Syst. **7**, 163 (2004).

[52] M. Kosmulski, P. Dahlsten, P. Prochniak, and J. B. Rosenholm, Colloids Surf., A **301**, 425 (2007).
[53] A. R. Studart, E. Amstad, and L. J. Gauckler, Langmuir **23**, 1081 (2007).
[54] P. Bhattacharya, S. K. Saha, A. Yadav, P. E. Phelan, and R. S. Prasher, J. Appl. Phys. **95**, 6492 (2004).
[55] J. Koo and C. Kleinstreuer, J. Nanopart. Res. **6**, 577 (2004).
[56] L. D. Landau and E. M. Lifshitz, *Electrodymanics of Continuous Media* (Nauka, Moscow, 1992).
[57] J. A. Aronovitz and D. R. Nelson, J. Phys. (France) **47**, 1445 (1986).
[58] R. Prasher, P. E. Phelan, and P. Bhattacharya, Nano Lett. **6**, 1529 (2006).
[59] C. W. Nan, R. Birringer, D. R. Clarke, and H. Gleiter, J. Appl. Phys. **81**, 6692 (1997).
[60] W. H. Press, B. P. Flannery, S. A. Teukolsky, and W. T. Vettrling, *Numerical Recipes in Fortran: The Art of Scientific Computing* (Cambridge University Press, New York 1992).
[61] D. P. H. Hasselman and L. F. Johnson, J. Compos. Mater. **21**, 508 (1987).
[62] Y. Benveniste, J. Appl. Phys. **61**, 2840 (1987).
[63] O. M. Wilson, X. Hu, D. G. Cahill, and P. V. Braun, Phys. Rev. B **66**, 224301 (2002).
[64] H. A. Patel, S. Garde, and P. Keblinski, Nano Lett. **5**, 2225 (2005).